

Deep inelastic (anti)neutrino-nucleus scattering

V. Ansari¹, M. Sajjad Athar¹, H. Haider^{1a}, I. Ruiz Simo², S. K. Singh¹ and F. Zaidi¹

¹Department of Physics, Aligarh Muslim University, Aligarh-202002, India

²Departamento de Física Atómica, Molecular y Nuclear, and Instituto de Física Teórica y Computacional Carlos I, Universidad de Granada, Granada 18071, Spain

Abstract. The present status of the field theoretical model studies of the deep inelastic scattering induced by (anti)neutrino on the nuclear targets in a wide range of Bjorken variable x and four momentum transfer square Q^2 , has been reviewed [1, 2, 3, 4, 5, 6]. The effect of the nonperturbative corrections such as target mass correction and higher twist effects, perturbative evolution of the parton densities, nuclear medium modifications in the nucleon structure functions, nuclear isoscalarity corrections on the weak nuclear structure functions have been discussed. These structure functions have been used to obtain the differential scattering cross sections. The various nuclear medium effects like the Fermi motion, binding energy, nucleon correlations, mesonic contributions, shadowing and antishadowing corrections relevant in the different regions of x and Q^2 have been discussed. The numerical results for the structure functions and the cross sections are compared with some of the available experimental data including the recent results from MINERvA. The predictions are made in argon nuclear target which is planned to be used as a target material in DUNE at the Fermilab.

1 Introduction

In recent years the need for a better understanding of neutrino interaction cross section with nucleon and nuclear targets in the few GeV region of (anti)neutrino energies has been emphasized in order to reduce the systematic uncertainty in the analysis of neutrino oscillation parameters of the Pontecorvo-Maki-Nakagawa-Sakata matrix (PMNS matrix). The lack in the understanding of (anti)neutrino-nucleon/nucleus cross section adds to 25-30% uncertainty to the systematics and a considerable reduction in this uncertainty is required for a precise measurement of PMNS matrix or in the study of CP violation in the leptonic sector or in the determination of the neutrino mass hierarchy (normal or inverted). In the few GeV region of (anti)neutrino energies the contribution to the total (anti)neutrino cross section comes from the quasielastic, inelastic as well as the deep inelastic scattering processes on the nuclear targets. In this review, we shall focus on the understanding of nuclear medium effects

^a email: huma.haider8@gmail.com

in the weak interaction induced deep inelastic scattering(DIS) processes in a theoretical model using field theory. For the details on the current status readers are referred to Ref.[7].

There is intrinsic interest to understand DIS processes induced by the charged leptons and (anti)neutrinos on nucleons and nuclear targets as they are important tools to study the quark parton structure of the free nucleons and the nucleons when they are bound in a nucleus. The observation of EMC (European Muon Collaboration) effect in the DIS of muon from iron target showed that the quark parton distributions of free nucleons are considerably modified when they are bound in a nucleus which was later confirmed in several other experiments by using electron, muon, (anti)neutrino and other particle beams on the various nuclear targets. The DIS experiments done with lepton beams make measurements of the DIS cross sections which are expressed in terms of the nucleon structure functions. These structure functions are determined by making Rosenbluth-like separations of the measured cross section. The electromagnetic DIS cross section induced by the charged leptons are generally expressed in terms of the two structure functions $F_{iN}^{EM}(x, Q^2)$ ($i = 1, 2$), which are functions of the Bjorken scaling variable $x = \frac{Q^2}{2M_N\nu}$ ($0 \leq x \leq 1$); and Q^2 (where $Q^2 \geq 0$, is the four momentum transfer square and ν is the energy transferred to the target i.e. $\nu = E_\nu - E_l$, $E_\nu(E_l)$ is the energy of the incoming(outgoing) lepton, and M_N is the nucleon mass). For the weak DIS process induced by (anti)neutrinos the cross sections are given in terms of three structure functions $F_{iN}^{Weak}(x, Q^2)$ ($i = 1, 2, 3$), in the limit of the vanishing lepton mass. However, in the case of DIS induced by the weak charged current of ν_μ and ν_τ , where the lepton mass in the final state could be non-negligible as compared to Q^2 in some kinematic regions, then two additional structure functions $F_{4N}^{Weak}(x, Q^2)$ and $F_{5N}^{Weak}(x, Q^2)$ also contribute to the cross sections. In the exact limit of Bjorken scaling i.e. $\nu \rightarrow \infty$, $Q^2 \rightarrow \infty$, such that $x = \frac{Q^2}{2M_N\nu}$, remains fixed, the structure functions scale and become functions of only one variable x . These structure functions are not all independent when calculated in the quark-parton model and satisfy certain relations given by Callan-Gross [8] and Albright-Jarlskog [9]. Consequently, the electromagnetic cross sections are given in terms of only one structure function chosen to be $F_{2N}^{EM}(x, Q^2)$ while the weak cross sections are given in terms of two structure functions taken to be $F_{2N}^{Weak}(x, Q^2)$ and $F_{3N}^{Weak}(x, Q^2)$.

The study of the nucleon structure functions gives important information about the structure of the nucleon and provides opportunity to test the predictions of the perturbative Quantum Chromodynamics(QCD). Depending upon the kinematic region of the centre of mass energy (W) and the four momentum transfer square(Q^2), it can also provide some important information about the non-perturbative QCD. In case of the electromagnetic(EM) DIS reactions induced by electrons and muons there is considerable experimental data on the EM nucleon structure functions viz. $F_{1N}^{EM}(x, Q^2)$ and $F_{2N}^{EM}(x, Q^2)$ and the nuclear structure functions $F_{1A}^{EM}(x, Q^2)$ and $F_{2A}^{EM}(x, Q^2)$ enabling us to study the nuclear medium effects on the electromagnetic nucleon structure functions by making a comparative study. This is not so in the case of weak nucleon structure function $F_{1N}^{Weak}(x, Q^2)$, $F_{2N}^{Weak}(x, Q^2)$ and $F_{3N}^{Weak}(x, Q^2)$, where there is almost no experimental data on free nucleons. The weak nucleon structure functions have to be extracted from the (anti)neutrino DIS experiment on heavy nuclear targets like freon, freon-propane, etc. MINERvA at Fermilab [10] has performed experiment with ν_μ and $\bar{\nu}_\mu$ beams in the wide range of x and Q^2 using several nuclear targets like carbon, iron, lead, etc. and the aim is to understand nuclear medium effects by doing EMC kind of measurements. Theoretically, a better understanding of nuclear medium effects on the weak structure functions is also required.

Generally there are two approaches in order to understand the medium effects in the weak nuclear structure functions, one is phenomenological and the other is theoretical. In the phenomenological analysis, the general approach is that nuclear parton distribution functions(PDFs) are obtained using the charged lepton-nucleus scattering data and analyzing the ratio of the structure functions e.g. $\frac{F_{2A}^{EM}}{F_{2A'}^{EM}}, \frac{F_{2A}^{EM}}{F_{2D}^{EM}}$, where A, A' represent any two nuclei and D stands for the deuteron, nuclear correction factor is determined. The same correction factor is then used for the weak structure functions $F_{1A}^{Weak}(x, Q^2)$ and $F_{2A}^{Weak}(x, Q^2)$. For $F_{3A}^{Weak}(x, Q^2)$, the information is inferred from (anti)neutrino scattering data [11,12,13]. The other phenomenological approach is to directly extract the nuclear PDFs by analyzing the experimental data i.e. without using nucleon PDFs or nuclear correction factor. This approach has been recently used by nCTEQ [14] group in getting $F_{2A}^{EM}(x, Q^2)$, $F_{2A}^{Weak}(x, Q^2)$ and $F_{3A}^{Weak}(x, Q^2)$ nuclear structure functions by analyzing together the charged lepton- A DIS data and Drell-Yan p - A data sets, and separately analyzing $\nu(\bar{\nu}) - A$ DIS data sets. Their observation is that the nuclear medium effects on $F_{2A}^{EM}(x, Q^2)$ in electromagnetic interaction are different from $F_{2A}^{Weak}(x, Q^2)$ in the weak interaction specially at low x .

On the other hand, theoretically, there have been very few calculations to study nuclear medium effects in the weak structure functions. One is by us (Aligarh-Valencia collaboration [1,2,3,4,5,6,15]), and the other is by Kulagin and Petti [16,17]. The present review is based on our theoretical works performed in the last several years [1, 2,3,4,5,6,15], on the electromagnetic and weak interaction induced DIS processes on the free nucleon and nuclear target in the wide region of x and Q^2 . Recently we have extended our study for $\nu_\tau/\bar{\nu}_\tau$ scattering on the free nucleon and obtained the structure functions as well as the differential and total scattering cross sections by including various perturbative and non-perturbative effects [6]. Work is in progress to understand nuclear medium effects in $\nu_\tau(\bar{\nu}_\tau)$ -nucleus interactions and will be reported elsewhere.

In the present paper, we review the work on the nuclear medium effects in the structure functions using a microscopic approach based on field theoretical formalism [18]. A relativistic nucleon spectral function has been used to describe the energy and momentum distribution of the nucleons in nuclei [19]. This is obtained by using the Lehmann's representation for the relativistic nucleon propagator and nuclear many body theory is used to calculate it for an interacting Fermi sea in nuclear matter. A local density approximation is then applied to translate these results to finite nuclei. Furthermore, we include the contributions of meson clouds and include the pion and rho contributions in a many body field theoretical approach. For the shadowing and anti-shadowing corrections which have been found to be effective in the low region of $x(x \leq 0.2)$, we follow the works of Kulagin and Petti [16,17]. In the present work the numerical results for various structure functions and the cross sections have been presented and compared with experiments. Predictions have been made for ^{40}Ar , relevant for the upcoming DUNE experiment[20] at the Fermilab.

The plan of the paper is the following. In section-2, we describe, in brief the formalism for calculating $\nu_l(\bar{\nu}_l)$ -nucleon scattering cross section and in section-3 we discuss the nuclear medium effects in the evaluation of structure functions and differential scattering cross section for $\nu_l(\bar{\nu}_l)$ -nucleus scattering. In section-4, we present and discuss the results and section-5, summarizes our study.

2 Formalism

2.1 (Anti)neutrino-nucleon cross section and the structure functions

The basic reaction for the (anti)neutrino induced charged current deep inelastic scattering process on a free nucleon target is given by

$$\nu_l(k)/\bar{\nu}_l(k) + N(p) \rightarrow l^-(k')/l^+(k') + X(p'); \quad l = e/\mu/\tau, \quad N = n, p, \quad (1)$$

where k and k' are the four momenta of incoming and outgoing lepton, p and p' are the four momenta of the target nucleon and the jet of hadrons produced in the final state, respectively. This process is mediated by the W -boson (W^\pm) and the invariant matrix element corresponding to the reaction given in Eq.1, is written as

$$-i\mathcal{M} = \frac{iG_F}{\sqrt{2}} l_\mu \left(\frac{M_W^2}{q^2 - M_W^2} \right) \langle X | J^\mu | N \rangle, \quad (2)$$

where G_F is the Fermi coupling constant, M_W is the mass of W boson, and $q^2 = (k - k')^2$ is the four momentum transfer square. l_μ is the leptonic current and $\langle X | J^\mu | N \rangle$ is the hadronic current for the neutrino induced reaction.

The general expression of the double differential scattering cross section (DCX) corresponding to the reaction given in Eq. 1 (depicted in Fig. 1) in the laboratory frame is expressed as:

$$\frac{d^2\sigma}{dx dy} = \frac{yM_N}{\pi} \frac{E_\nu}{E_l} \frac{|k'|}{|k|} \frac{G_F^2}{2} \left(\frac{M_W^2}{Q^2 + M_W^2} \right)^2 L_{\mu\nu} W_N^{\mu\nu}, \quad (3)$$

where x and y are the scaling variables which lie in the following ranges:

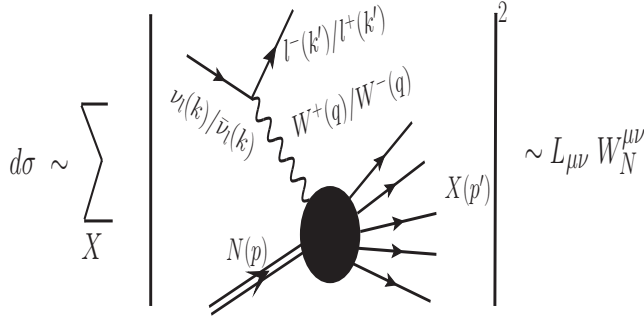


Fig. 1. $\nu_l(\bar{\nu}_l) - N$ inclusive scattering, where the summation sign represents the sum over all the hadronic states such that the cross section($d\sigma$) for the deep inelastic scattering $\propto L_{\mu\nu}W_N^{\mu\nu}$.

$$\frac{m_l^2}{2M_N(E_\nu - m_l)} \leq x \leq 1; \quad a - b \leq y \leq a + b, \quad (4)$$

with

$$a = \frac{1 - m_l^2 \left(\frac{1}{2M_N E_\nu x} + \frac{1}{2E_\nu^2} \right)}{2 \left(1 + \frac{M_N x}{2E_\nu} \right)}, \quad b = \frac{\sqrt{\left(1 - \frac{m_l^2}{2M_N E_\nu x} \right)^2 - \frac{m_l^2}{E_\nu^2}}}{2 \left(1 + \frac{M_N x}{2E_\nu} \right)}, \quad (5)$$

where m_l is the charged lepton mass. The leptonic tensor $L_{\mu\nu}$ is given by

$$L_{\mu\nu} = 8(k_\mu k'_\nu + k_\nu k'_\mu - k \cdot k' g_{\mu\nu} \pm i\epsilon_{\mu\nu\rho\sigma} k^\rho k'^\sigma), \quad (6)$$

with +ve sign for antineutrino and -ve sign for neutrino in the antisymmetric term.

The hadronic tensor $W_N^{\mu\nu}$ is written in terms of the weak nucleon structure functions $W_{iN}(\nu, Q^2)$ ($i = 1 - 6$) as

$$\begin{aligned} W_N^{\mu\nu} &= \left(\frac{q^\mu q^\nu}{q^2} - g^{\mu\nu} \right) W_{1N}(\nu, Q^2) + \frac{W_{2N}(\nu, Q^2)}{M_N^2} \left(p^\mu - \frac{p \cdot q}{q^2} q^\mu \right) \\ &\times \left(p^\nu - \frac{p \cdot q}{q^2} q^\nu \right) - \frac{i}{2M_N^2} \epsilon^{\mu\nu\rho\sigma} p_\rho q_\sigma W_{3N}(\nu, Q^2) + \frac{W_{4N}(\nu, Q^2)}{M_N^2} q^\mu q^\nu \\ &+ \frac{W_{5N}(\nu, Q^2)}{M_N^2} (p^\mu q^\nu + q^\mu p^\nu) + \frac{i}{M_N^2} (p^\mu q^\nu - q^\mu p^\nu) W_{6N}(\nu, Q^2). \end{aligned} \quad (7)$$

The contribution of the term with $W_{6N}(\nu, Q^2)$ vanishes when contracted with the leptonic tensor. In the limit of high Q^2 and ν , the structure functions $W_{iN}(\nu, Q^2)$; ($i = 1 - 5$) are generally expressed in terms of the dimensionless nucleon structure functions $F_{iN}(x)$, $i = 1 - 5$. However, as we move towards the region of low and moderate Q^2 , the dimensionless nucleon structure functions show x as well as Q^2 dependence. Hence, $F_{iN}(x, Q^2)$, $i = 1 - 5$ are defined as

$$\begin{aligned} F_{1N}(x, Q^2) &= W_{1N}(\nu, Q^2), \quad F_{2N}(x, Q^2) = \frac{Q^2}{2xM_N^2} W_{2N}(\nu, Q^2), \quad F_{3N}(x, Q^2) = \frac{Q^2}{xM_N^2} W_{3N}(\nu, Q^2), \\ F_{4N}(x, Q^2) &= \frac{Q^2}{2M_N^2} W_{4N}(\nu, Q^2), \quad F_{5N}(x, Q^2) = \frac{Q^2}{2xM_N^2} W_{5N}(\nu, Q^2). \end{aligned} \quad (8)$$

The expression for the differential scattering cross section for the $\nu_l/\bar{\nu}_l - N$ scattering given in Eq. 3 is written by using Eqs. 6 and 8 as:

$$\begin{aligned} \frac{d^2\sigma}{dx dy} &= \frac{G_F^2 M_N E_\nu}{\pi(1 + \frac{Q^2}{M_W^2})^2} \left\{ \left[y^2 x + \frac{m_l^2 y}{2E_\nu M_N} \right] F_{1N}(x, Q^2) + \left[\left(1 - \frac{m_l^2}{4E_\nu^2} \right) - \left(1 + \frac{M_N x}{2E_\nu} \right) y \right] F_{2N}(x, Q^2) \right. \\ &\left. \pm \left[xy \left(1 - \frac{y}{2} \right) - \frac{m_l^2 y}{4E_\nu M_N} \right] F_{3N}(x, Q^2) + \frac{m_l^2 (m_l^2 + Q^2)}{4E_\nu^2 M_N^2 x} F_{4N}(x, Q^2) - \frac{m_l^2}{E_\nu M_N} F_{5N}(x, Q^2) \right\}. \end{aligned} \quad (9)$$

In general, the dimensionless nucleon structure functions are derived in the quark-parton model assuming Bjorken scaling in which they scale and are functions of only one variable x . In this limit, these structure functions obey Callan-Gross [8] and Albright-Jarlskog [9] relations

$$F_1(x) = \frac{F_2(x)}{2x}; \quad F_5(x) = \frac{F_2(x)}{2x},$$

and at the leading order, the structure functions are written in terms of the parton distribution functions $q_i(x)$ and $\bar{q}_i(x)$ as:

$$F_2(x) = \sum_i x[q_i(x) + \bar{q}_i(x)]; \quad xF_3(x) = \sum_i x[q_i(x) - \bar{q}_i(x)]; \quad F_4(x) = 0. \quad (10)$$

For example, in the case of $\nu(\bar{\nu})$ -proton scattering above the charm production threshold, $F_{2,3}(x)$ are given by:

$$\begin{aligned} F_{2p}^\nu(x) &= 2x[d(x) + s(x) + \bar{u}(x) + \bar{c}(x)]; \quad F_{2p}^{\bar{\nu}}(x) = 2x[u(x) + c(x) + \bar{d}(x) + \bar{s}(x)]; \\ xF_{3p}^\nu(x) &= 2x[d(x) + s(x) - \bar{u}(x) - \bar{c}(x)]; \quad xF_{3p}^{\bar{\nu}}(x) = 2x[u(x) + c(x) - \bar{d}(x) - \bar{s}(x)] \end{aligned} \quad (11)$$

and for the $\nu(\bar{\nu})$ -neutron scattering $F_{2,3}(x)$ are given by

$$\begin{aligned} F_{2n}^\nu(x) &= 2x[u(x) + s(x) + \bar{d}(x) + \bar{c}(x)]; & F_{2n}^{\bar{\nu}}(x) &= 2x[d(x) + c(x) + \bar{u}(x) + \bar{s}(x)]; \\ xF_{3n}^\nu(x) &= 2x[u(x) + s(x) - \bar{d}(x) - \bar{c}(x)]; & xF_{3n}^{\bar{\nu}}(x) &= 2x[d(x) + c(x) - \bar{u}(x) - \bar{s}(x)]. \end{aligned} \quad (12)$$

For an isoscalar nucleon target, we use

$$F_{iN} = \frac{F_{ip} + F_{in}}{2}. \quad (i = 1 - 5) \quad (13)$$

In the present formalism we have performed numerical calculations in the three(u , d and s) as well as four(u , d , s and c) flavor schemes by taking u , d and s to be massless and the charm quark to be massless as well as massive. In the region of low and moderate Q^2 , the perturbative and nonperturbative QCD corrections such as Q^2 evolution of parton distribution functions from leading order to higher order terms (next-to-leading order (NLO), next-next-to-leading order (NNLO), ...), the effects of target mass correction due to the massive quarks production (e.g. charm, bottom, top) and higher twist (twist-4, twist-6, ...) because of the multiparton correlations, become important. These nonperturbative effects are specifically important in the kinematical region of high x and low Q^2 . The Q^2 evolution of structure functions is determined by the DGLAP evolution equation [21, 22, 23, 24]. The parton distribution functions for the nucleon have been determined by various groups and we have taken the parameterization of MMHT [25] in our numerical calculations up to NNLO following Ref. [26, 27, 28]. The nonperturbative higher twist effect is incorporated by using the renormalon approach [29] and the target mass correction is included following the works of Schienbein et al. [30]. The incorporation of the contribution from gluon emission induces the Q^2 dependence of the nucleon structure functions. The details of the discussion are given in Ref. [5].

2.2 (Anti)neutrino-nucleus cross section and structure functions

The differential scattering cross section for the charged current inclusive $\nu_l/\bar{\nu}_l$ -nucleus deep inelastic scattering process (depicted in Fig. 2):

$$\nu_l/\bar{\nu}_l(k) + A(p_A) \rightarrow l^-/l^+(k') + X(p'_A) \quad (14)$$

is expressed in terms of the leptonic tensor $L_{\mu\nu}$ and the nuclear hadronic tensor $W_A^{\mu\nu}$ as:

$$\frac{d^2\sigma_A}{dx dy} = \left(\frac{G_F^2 y M_N E_\nu}{2\pi E_l} \right) \left(\frac{M_W^2}{M_W^2 + Q^2} \right)^2 \frac{|\mathbf{k}'|}{|\mathbf{k}|} L_{\mu\nu} W_A^{\mu\nu}, \quad (15)$$

where the physical quantities have their usual meanings. The expression of $L_{\mu\nu}$ is given by Eq.6. The nuclear hadronic tensor $W_A^{\mu\nu}$ is written in terms of the weak nuclear structure functions $W_{iA}(\nu_A, Q^2)$ ($i = 1 - 6$) as:

$$\begin{aligned} W_A^{\mu\nu} &= \left(\frac{q^\mu q^\nu}{q^2} - g^{\mu\nu} \right) W_{1A}(\nu_A, Q^2) + \frac{W_{2A}(\nu_A, Q^2)}{M_A^2} \left(p_A^\mu - \frac{p_A \cdot q}{q^2} q^\mu \right) \\ &\times \left(p_A^\nu - \frac{p_A \cdot q}{q^2} q^\nu \right) \pm \frac{i}{2M_A^2} \epsilon^{\mu\nu\rho\sigma} p_{A\rho} q_\sigma W_{3A}(\nu_A, Q^2) + \frac{W_{4A}(\nu_A, Q^2)}{M_A^2} q^\mu q^\nu \\ &+ \frac{W_{5A}(\nu_A, Q^2)}{M_A^2} (p_A^\mu q^\nu + q^\mu p_A^\nu) + \frac{i}{M_A^2} (p_A^\mu q^\nu - q^\mu p_A^\nu) W_{6A}(\nu_A, Q^2), \end{aligned} \quad (16)$$

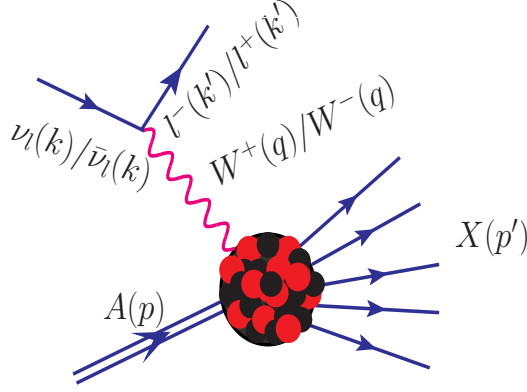


Fig. 2. Feynman diagrams for the $\nu_l/\bar{\nu}_l$; ($l = e, \mu, \tau$) induced DIS process off nuclear target (A).

where M_A is the mass of the nuclear target. The nuclear structure functions $W_{iA}(\nu_A, Q^2)$ ($i = 1-5$) are written in terms of the dimensionless nuclear structure functions $F_{iA}(x_A, Q^2)$ ($i = 1-5$) as:

$$\begin{aligned} F_{1A}(x_A, Q^2) &= W_{1A}(\nu_A, Q^2); & F_{2A}(x_A, Q^2) &= \frac{Q^2}{2xM_A^2}W_{2A}(\nu_A, Q^2); & F_{3A}(x_A, Q^2) &= \frac{Q^2}{xM_A^2}W_{3A}(\nu_A, Q^2); \\ F_{4A}(x_A, Q^2) &= \frac{Q^2}{2M_A^2}W_{4A}(\nu_A, Q^2); & F_{5A}(x_A, Q^2) &= \frac{Q^2}{2xM_A^2}W_{5A}(\nu_A, Q^2), \end{aligned} \quad (17)$$

where $\nu_A (= \frac{p_A \cdot q}{M_A} (= q^0))$ is the energy transferred to the target in the Lab frame and $x_A (= x/A)$ is the Bjorken scaling variable given by:

$$x_A = \frac{Q^2}{2p_A \cdot q} = \frac{Q^2}{2p_A^0 q^0} = \frac{Q^2}{2A M_N q^0} = \frac{x}{A}. \quad (18)$$

The expression for the differential cross section for the $\nu_l/\bar{\nu}_l - A$ scattering can be obtained using Eqs. 6, 16 and 17 in Eq. 15 as

$$\begin{aligned} \frac{d^2\sigma_A}{dx dy} &= \frac{G_F^2 M_N E_\nu}{\pi(1 + \frac{Q^2}{M_W^2})^2} \left\{ \left[y^2 x + \frac{m_l^2 y}{2E_\nu M_N} \right] F_{1A}(x, Q^2) + \left[\left(1 - \frac{m_l^2}{4E_\nu^2} \right) - \left(1 + \frac{M_N x}{2E_\nu} \right) y \right] F_{2A}(x, Q^2) \right. \\ &\quad \left. \pm \left[xy \left(1 - \frac{y}{2} \right) - \frac{m_l^2 y}{4E_\nu M_N} \right] F_{3A}(x, Q^2) + \frac{m_l^2 (m_l^2 + Q^2)}{4E_\nu^2 M_N^2 x} F_{4A}(x, Q^2) - \frac{m_l^2}{E_\nu M_N} F_{5A}(x, Q^2) \right\}. \end{aligned} \quad (19)$$

For $\nu_e/\bar{\nu}_e$ and $\nu_\mu/\bar{\nu}_\mu$ charged current interactions, in the limit $m_l \rightarrow 0$, only the first three terms of Eq. 19, i.e. the terms with $F_{1A}(x, Q^2)$, $F_{2A}(x, Q^2)$ and $F_{3A}(x, Q^2)$ structure functions would contribute. We consider the scattering process in the laboratory frame, where target nucleus is at rest i.e. $p_A = (p_A^0, \mathbf{p}_A = 0)$ and the momentum of the nucleon in the nucleus (\mathbf{p}_N) is non-zero and the motion of such nucleons corresponds to the Fermi motion.

If the momentum transfer is along the Z -axis then $q^\mu = (q^0, 0, 0, q^z)$ and the Bjorken variable x_N is written as:

$$x_N = \frac{Q^2}{2p_N \cdot q} = \frac{Q^2}{2(p_N^0 q^0 - p_N^z q^z)}. \quad (20)$$

The nuclear medium effects such as Fermi motion, binding, nucleon correlations incorporated through nucleon spectral function, meson cloud contribution and shadowing effect are discussed in the following subsections 2.2.1, 2.2.2 and 2.2.3.

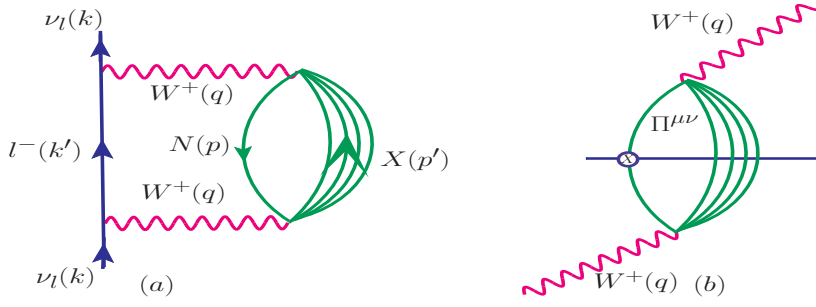


Fig. 3. Diagrammatic representation of (a) the neutrino (ν_l) self-energy and (b) the intermediate vector boson (W) self-energy.

2.2.1 Effect of Fermi motion, binding and nucleon correlation

We start by writing the scattering cross section ($d\sigma_A$) for small elemental volume (dV) inside the nucleus in terms of the probability of neutrino interaction with a bound nucleon per unit time (Γ). Probability times the differential of area (dS) defines the cross section [18], i.e.

$$d\sigma_A = \Gamma dt dS = \Gamma \frac{E_\nu}{|\mathbf{k}|} d^3 r, \quad \left[\because dt dS = \frac{dV}{v} = \frac{E_\nu}{|\mathbf{k}|} d^3 r \right] \quad (21)$$

where v is the velocity of the incoming neutrino. Γ is related to the imaginary part of the ν_l self energy ($\Sigma(k)$) as [18]:

$$-\frac{\Gamma}{2} = \frac{m_\nu}{E_\nu(\mathbf{k})} \text{Im}\Sigma(k). \quad (22)$$

It may be pointed out that the neutrino self energy $\Sigma(k)$ has two parts, the real part of “neutrino self energy” modifies the lepton mass and imaginary part i.e. $\text{Im}\Sigma(k)$ gives information about the total number of neutrinos interactions that yield the final state leptons and hadrons.

From Eq.21 and Eq.22, we get

$$d\sigma_A = -2 \frac{m_\nu}{|\mathbf{k}|} \text{Im}\Sigma(k) d^3 r. \quad (23)$$

$\Sigma(k)$ is evaluated corresponding to the diagram shown in Fig.3 (left panel) using the Feynman rules and on applying the Cutkowsky rules the imaginary part of neutrino self energy is obtained as [3]:

$$\text{Im}\Sigma(k) = \frac{G_F}{\sqrt{2}} \frac{4}{m_\nu} \int \frac{d^3 k'}{(2\pi)^4} \frac{\pi}{E(\mathbf{k}')} \theta(q^0) \left(\frac{M_W}{Q^2 + M_W^2} \right)^2 \text{Im}[L_{\mu\nu}^{WI} \Pi^{\mu\nu}(q)], \quad (24)$$

where $\Pi^{\mu\nu}(q)$ is the W -boson self-energy (as shown in Fig. 3(b)), which is generally written in terms of the nucleon propagator (G_i) and meson propagator (D_j) corresponding to Fig. 3(b), as:

$$\begin{aligned} \Pi^{\mu\nu}(q) &= \left(\frac{G_F M_W^2}{\sqrt{2}} \right) \times \int \frac{d^4 p}{(2\pi)^4} G(p) \sum_X \sum_{s_p, s_l} \prod_{i=1}^N \int \frac{d^4 p'_i}{(2\pi)^4} \prod_l G_l(p'_l) \prod_j D_j(p'_j) \\ &< X | J^\mu | N \rangle \langle X | J^\nu | N \rangle^* (2\pi)^4 \delta^4 \left(k + p - k' - \sum_{i=1}^N p'_i \right), \end{aligned} \quad (25)$$

where s_p and s_l are the spin of the initial state nucleon and the final state fermions, the indices l and j are respectively, for the fermions and bosons in the final hadronic state, $\langle X|J^\mu|N \rangle$ represents the hadronic current and $\delta^4(k + p - k' - \sum_{i=1}^N p'_i)$ ensures the conservation of four momentum. $G(p)$ gives the information about the propagation of the nucleon from the initial state to the final state or vice versa.

To obtain the relativistic nucleon propagator $G(p^0, \mathbf{p})$ in a nuclear medium we start with the relativistic free nucleon Dirac propagator $G^0(p^0, \mathbf{p})$ which is written in terms of the Dirac spinors $u(\mathbf{p})$ and $v(\mathbf{p})$. This includes the contribution from positive and negative energy components of the nucleon and the negative energy contribution is suppressed while the positive energy contribution survives [18, 19]. Considering only the positive energy part of the nucleon propagator $G^0(p^0, \mathbf{p})$, we write

$$G^0(p^0, \mathbf{p}) = \frac{\not{p} + M_N}{p^2 - M_N^2 + i\epsilon} + 2 i\pi\theta(p^0)\delta(p^2 - M_N^2)n(\mathbf{p})(\not{p} + M_N). \quad (26)$$

In the nuclear medium considered as an interacting Fermi sea, $G(p^0, \mathbf{p})$ is written in terms of the nucleon self energy $\Sigma^N(p^0, \mathbf{p})$, which contains all the information on single nucleon. Then in nuclear medium the interaction is taken into account through Dyson series expansion, which is in principle an infinite series in perturbation theory. This perturbative expansion is summed in a ladder approximation as [18]:

$$G(p) = \frac{M_N}{E(\mathbf{p})} \frac{\sum_r u_r(\mathbf{p})\bar{u}_r(\mathbf{p})}{p^0 - E(\mathbf{p}) - \sum_r \bar{u}_r(\mathbf{p})\Sigma^N(p^0, \mathbf{p})u_r(\mathbf{p})\frac{M_N}{E(\mathbf{p})}}. \quad (27)$$

One may notice from the expression for the nucleon propagator $G(p)$ given in Eq.27 that it contains nucleon self energy $\Sigma^N(p^0, \mathbf{p})$. The nucleon self-energy is written using the techniques of the standard Many-Body Theory [19]. The inputs required for the NN interaction are incorporated by relating them to the experimental elastic NN cross section. Furthermore, RPA-correlation effect is taken into account using the spin-isospin effective interaction as the dominating part of the particle-hole (ph) interaction. Using the modified expression for the nucleon self energy, the imaginary part of it is obtained [31]. These considerations lead to a dressed nucleon propagator in the nuclear matter which is given by [18,19]:

$$G(p) = \frac{M_N}{E(\mathbf{p})} \sum_r u_r(\mathbf{p})\bar{u}_r(\mathbf{p}) \left[\int_{-\infty}^{\mu} d\omega \frac{S_h(\omega, \mathbf{p})}{p^0 - \omega - i\eta} + \int_{\mu}^{\infty} d\omega \frac{S_p(\omega, \mathbf{p})}{p^0 - \omega + i\eta} \right], \quad (28)$$

where the expressions for the hole $S_h(\omega, \mathbf{p})$ (for $p_0 \leq \mu$) and the particle $S_p(\omega, \mathbf{p})$ (for $p_0 \geq \mu$) spectral functions and the nucleon self energy $\Sigma^N(p^0, \mathbf{p})$ are taken from Ref. [19]. For an inclusive process, only the hole spectral function contributes. In the above expression, μ is the chemical potential given by $\mu = \frac{p_F^2}{2M} + Re\Sigma^N\left[\frac{p_F^2}{2M}, p_F\right]$ and $\omega = p^0 - M_N$ is the removal energy. η is the infinitesimal quantity i.e. $\eta \rightarrow 0$. p_F is the Fermi momentum of the nucleon in the nucleus. In the local Fermi gas model the Fermi momentum is a function r , the point at which the interaction in the nucleus takes place and is given by $p_F(r) = \left[\frac{3}{2}\pi^2\rho(r)\right]^{1/3}$, where $\rho(r)$ is the nucleon charge density inside the nucleus, the parameters of which are determined from electron scattering experiments [32]. The spectral function for an isoscalar nuclear target is normalized to the number of nucleons (A) in the nucleus i.e.

$$4 \int d^3r \int \frac{d^3p}{(2\pi)^3} \int_{-\infty}^{\mu} S_h(\omega, \mathbf{p}, \rho(r)) d\omega = A. \quad (29)$$

Some of the properties of the spectral function may be found in the appendix of Ref. [31].

Then using Eqs. 23 and 24 the expression for the differential cross section is written as

$$\frac{d\sigma_A}{dx dy} = -\frac{G_F^2 M_N y}{2\pi} \frac{E_l}{E_\nu} \frac{|\mathbf{k}'|}{|\mathbf{k}|} \left(\frac{M_W^2}{Q^2 + M_W^2} \right)^2 L_{\mu\nu} \int \text{Im} \Pi^{\mu\nu}(q) d^3 r. \quad (30)$$

Comparing Eq.30, with Eqs.15, 25 and 28, the nuclear hadronic tensor (for isospin symmetric nucleus) can be expressed in terms of the nucleon hadronic tensor and the hole spectral function and is given as [31]

$$W_A^{\mu\nu} = 4 \int d^3 r \int \frac{d^3 p}{(2\pi)^3} \frac{M_N}{E(\mathbf{p})} \int_{-\infty}^{\mu} dp^0 S_h(p^0, \mathbf{p}, \rho(r)) W_N^{\mu\nu}(p, q), \quad (31)$$

a factor of 4 is because of the spin-isospin degrees of freedom of the nucleon.

For a non-isoscalar nuclear target like ^{56}Fe and ^{208}Pb , the spectral functions for the proton (Z) and neutron ($N = A - Z$) numbers in a nuclear target which are the function of local Fermi momenta $p_{F_{p,n}}(r) = [3\pi^2 \rho_{p(n)}(r)]^{1/3}$, are normalized separately such that

$$2 \int d^3 r \int \frac{d^3 p}{(2\pi)^3} \int_{-\infty}^{\mu_p} S_h^p(\omega, \mathbf{p}, \rho_p(r)) d\omega = Z, \quad (32)$$

$$2 \int d^3 r \int \frac{d^3 p}{(2\pi)^3} \int_{-\infty}^{\mu_n} S_h^n(\omega, \mathbf{p}, \rho_n(r)) d\omega = N, \quad (33)$$

where the factor of 2 is due to the two possible projections of nucleon spin, μ_p (μ_n) is the chemical potential for the proton (neutron), and $S_h^p(\omega, \mathbf{p}, \rho_p(r))$ and $S_h^n(\omega, \mathbf{p}, \rho_n(r))$ are the hole spectral functions for the proton and neutron, respectively. The proton and neutron densities $\rho_p(r)$ and $\rho_n(r)$ are related to the nuclear density $\rho(r)$ as [3, 31]:

$$\rho_p(r) = \frac{Z}{A} \rho(r); \quad \rho_n(r) = \frac{(A - Z)}{A} \rho(r).$$

Hence for a nonisoscalar nuclear target, the nuclear hadronic tensor is written as

$$W_A^{\mu\nu} = 2 \sum_{\tau=p,n} \int d^3 r \int \frac{d^3 p}{(2\pi)^3} \frac{M_N}{E_N(\mathbf{p})} \int_{-\infty}^{\mu_\tau} dp^0 S_h^\tau(p^0, \mathbf{p}, \rho_\tau(r)) W_\tau^{\mu\nu}(p, q). \quad (34)$$

To evaluate the weak dimensionless nuclear structure functions by using Eq.31, the appropriate components of nucleon ($W_N^{\mu\nu}$ in Eq.7) and nuclear ($W_A^{\mu\nu}$ in Eq.16) hadronic tensors along the x , y and z axis are chosen. For example, the expression of $F_{1A,N}(x_A, Q^2)$ is obtained by taking the xx components, $F_{2A,N}(x_A, Q^2)$ by taking the zz components, $F_{3A,N}(x_A, Q^2)$ by taking the xy components, etc. [5], and for an isoscalar nuclear target, the expressions for the three nuclear structure functions viz. $F_{iA,N}(x_A, Q^2)$ $i = 1 - 3$ i.e. for the massless leptons as are obtained as:

$$F_{iA,N}(x_A, Q^2) = 4 \int d^3 r \int \frac{d^3 p}{(2\pi)^3} \frac{M_N}{E_N(\mathbf{p})} \int_{-\infty}^{\mu} dp^0 S_h(p^0, \mathbf{p}, \rho(r)) \times f_{iN}(x, Q^2), \quad (35)$$

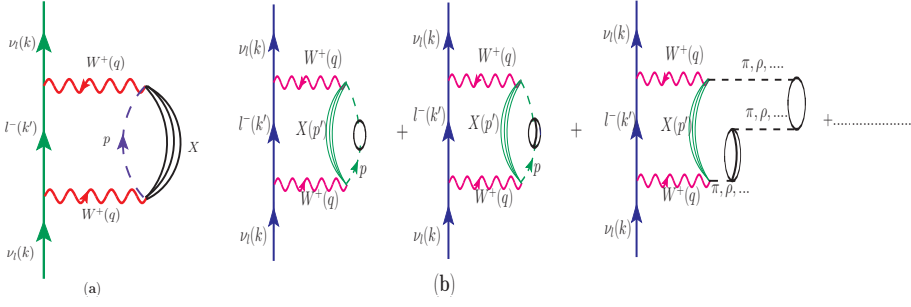


Fig. 4. Neutrino self energy diagram accounting for neutrino-meson DIS (a) the bound nucleon propagator is substituted with a meson(π or ρ) propagator with momentum p represented here by dashed line (b) by including particle-hole ($1p-1h$), delta-hole ($1\Delta-1h$), $1p1h - 1\Delta1h$, etc. interactions.

where

$$f_{1N}(x, Q^2) = AM_N \left[\frac{F_{1N}(x_N, Q^2)}{M_N} + \left(\frac{p^x}{M_N} \right)^2 \frac{F_{2N}(x_N, Q^2)}{\nu_N} \right], \quad (36)$$

$$f_{2N}(x, Q^2) = \left[\frac{Q^2}{(q^z)^2} \left(\frac{|\mathbf{p}|^2 - (p^z)^2}{2M_N^2} \right) + \frac{(p^0 - p^z \gamma)^2}{M_N^2} \left(\frac{p^z Q^2}{(p^0 - p^z \gamma)q^0 q^z} + 1 \right)^2 \right] \times \left(\frac{M_N}{p^0 - p^z \gamma} \right) \times F_{2N}(x_N, Q^2), \quad (37)$$

$$f_{3N}(x, Q^2) = A \frac{q^0}{q^z} \times \left(\frac{p^0 q^z - p^z q^0}{p \cdot q} \right) F_{3N}(x_N, Q^2). \quad (38)$$

Similar expression is obtained for a non-isoscalar nuclear target [5].

The nonperturbative effects of the target mass corrections and the higher twist [29] have been incorporated in the free nucleon structure functions and then we have convoluted these nucleon structure functions with the spectral function in order to evaluate the nuclear structure functions (Eq.35). Using the nuclear structure functions, we have obtained the differential scattering cross sections for the $\nu_l(\bar{\nu}_l) - A$, $l = e, \mu$ DIS process (Eq.19).

The calculations are performed in the four flavor MS-bar scheme. We have considered two cases: (i) In the case of massless leptons (e^\pm, μ^\pm), all the four quarks, i.e., u, d, s and c are treated to be massless while (ii) For massive lepton (τ^\pm), light quarks u, d and s are treated as massless but charm quark c as a massive object for which we define

$$F_{iA}(x, Q^2) = F_{iA}^{n_f=4}(x, Q^2) = \underbrace{F_{iA}^{n_f=3}(x, Q^2)}_{\text{for massless}(u, d, s) \text{ quarks}} + \underbrace{F_{iA}^{n_f=1}(x, Q^2)}_{\text{for massive charm quark}}. \quad (39)$$

The nucleons which are bound inside the nucleus may interact with each other via meson exchange such as π, ρ , etc. This mesonic effect has been incorporated and is discussed in the next sub-subsection 2.2.2.

2.2.2 Effect of mesonic cloud contribution

Associated with each bound nucleon there are virtual mesons (pion, rho meson, etc.) and because of the strong attractive nature of the nucleon-nucleon interaction, the

probability of a W -boson interaction with the mesonic cloud becomes high. We have discussed the π and ρ meson contributions in our earlier works [3,4,5,31,33]. The contribution from heavier mesons like ω meson are expected to be very small due to their significantly higher masses. The mesonic contribution is significant in the intermediate region of x ($0.2 < x < 0.6$). For the medium nuclei like ${}^4\text{He}$, ${}^{12}\text{C}$, etc., mesonic contribution is small [34] while it becomes pronounced in heavier nuclear targets [2] such as ${}^{56}\text{Fe}$, ${}^{208}\text{Pb}$, etc. To incorporate the mesonic effect we draw a diagram similar to Fig.3, but here a nucleon propagator is replaced by a meson propagator. The meson propagator corresponds to the virtual mesons arising due to the nuclear medium effects and can arise through the particle-hole ($1p-1h$), delta-hole ($1\Delta-1h$), $2p-2h$, etc. interactions as shown in Fig.4 [19].

The mesonic structure functions $F_{iA,a}(x_a, Q^2)$, ($i = 1, 2; a = \pi, \rho$) are obtained as [5]:

$$F_{iA,a}(x_a, Q^2) = -6\kappa \int d^3r \int \frac{d^4p}{(2\pi)^4} \theta(p^0) \delta Im D_a(p) 2m_a f_{ia}(x_a), \quad (40)$$

where

$$f_{1a}(x_a) = AM_N \left[\frac{F_{1a}(x_a)}{m_a} + \frac{|\mathbf{p}|^2 - (p^z)^2}{2(p^0 q^0 - p^z q^z)} \frac{F_{2a}(x_a)}{m_a} \right], \quad (41)$$

$$f_{2a}(x_a) = \left[\frac{Q^2}{(q^z)^2} \left(\frac{|\mathbf{p}|^2 - (p^z)^2}{2m_a^2} \right) + \frac{(p^0 - p^z \gamma)^2}{m_a^2} \times \left(\frac{p^z Q^2}{(p^0 - p^z \gamma)q^0 q^z} + 1 \right)^2 \right] \times \left(\frac{m_a}{p^0 - p^z \gamma} \right) F_{2a}(x_a). \quad (42)$$

In Eqs. 40 and 41, $\kappa = 1(2)$ for pion(rho meson), $\nu = \frac{q_0(\gamma p^z - p^0)}{m_a}$, $x_a = -\frac{Q^2}{2p \cdot q}$, m_a is the mass of the meson(π or ρ). $D_a(p)$ is the meson(π or ρ) propagator in the nuclear medium and is written as

$$D_a(p) = [p_0^2 - \mathbf{p}^2 - m_a^2 - \Pi_a(p_0, \mathbf{p})]^{-1}, \quad (43)$$

with

$$\Pi_a(p_0, \mathbf{p}) = \frac{f^2}{m_\pi^2} \frac{C_\rho F_a^2(p) \mathbf{p}^2 \Pi^*}{1 - \frac{f^2}{m_\pi^2} V_j^I \Pi^*}, \quad (44)$$

where $C_\rho = 1(3.94)$ for pion(rho meson). $F_a(p) = \frac{(A_a^2 - m_a^2)}{(A_a^2 - p^2)}$ is the πNN or ρNN form factor, $A_a = 1 \text{ GeV}$ [15,31] and $f = 1.01$. V_j^I is the longitudinal(transverse) part of the spin-isospin interaction for pion(rho meson), and Π^* is the irreducible meson self energy that contains the contribution of particle-hole and delta-hole excitations. For the pions, we have used the PDFs parameterization given by Gluck et al.[35] and for the ρ mesons same PDFs as for the pions have been used as there is no available explicit parameterization for the ρ -meson PDFs in the literature.

2.2.3 Shadowing and Antishadowing effects

In this work the shadowing and antishadowing effects are taken into consideration following the works of Kulagin and Petti [16,17] who have used the original Glauber-Gribov multiple scattering theory. For example, with these effects, the nuclear structure function is given by

$$F_{iA,shd}(x, Q^2) = \delta R(x, Q^2) \times F_{iN}^{WI}(x, Q^2) \quad i = 1 - 3, \quad (45)$$

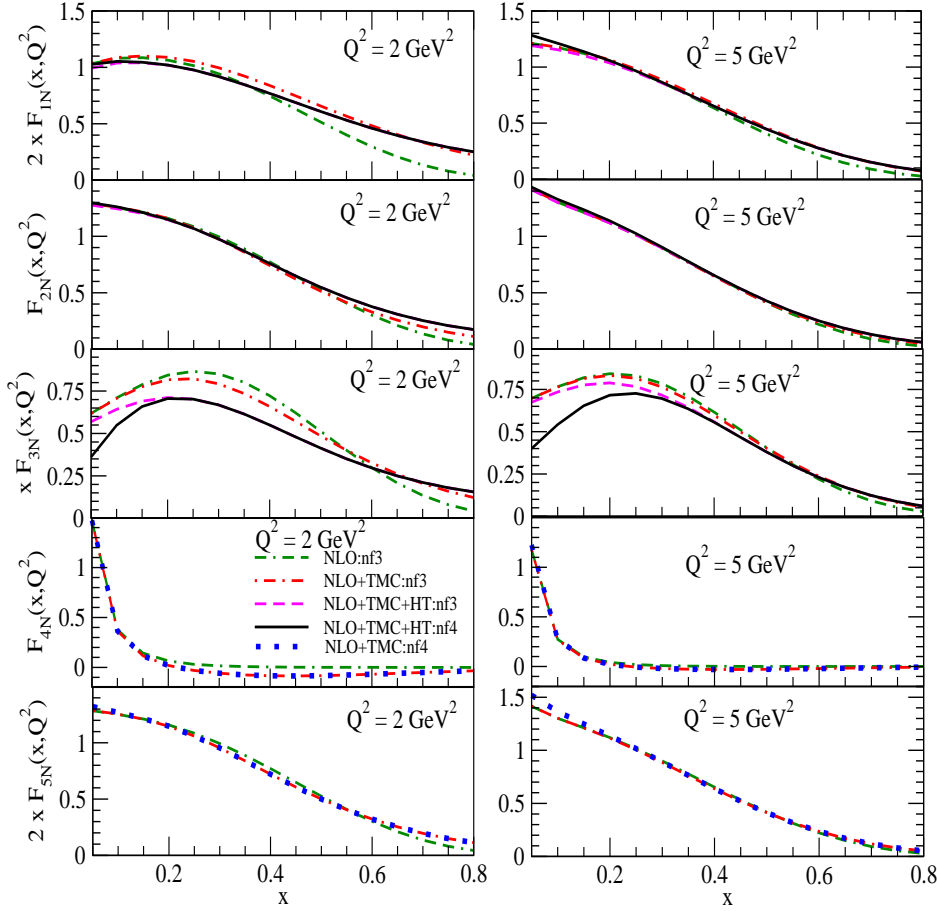


Fig. 5. Results for the free nucleon weak structure functions $F_{iN}(x, Q^2); (i = 1 - 5)$ (Top to Bottom) at the different values of $Q^2 = 2 \text{ GeV}^2$ (Left) and 5 GeV^2 (Right) are shown. These results are obtained at NLO by using MMHT nucleon PDFs parameterization [25]. The results are shown without the TMC effect (double dashed-dotted line), with the TMC effect in the 3-flavor(nf3) scheme (dashed-dotted line) as well as four flavor(nf4) scheme(dotted line), with TMC and HT effects in the 3-flavor(nf3) scheme (dashed line) as well as four flavor(nf4) scheme(solid line).

where the expression for $\delta R(x, Q^2)$ used in the present numerical calculations is given in Ref. [17].

Now, using the present formalism, we have presented the results for the weak structure functions and scattering cross sections for both the free nucleon and nuclear targets in the next section.

3 Results and Discussion

First, we present the results for the free nucleon weak structure functions $F_{iN}(x, Q^2); (i = 1 - 5)$, and using them the results for the total scattering cross section $\sigma(E_\nu)$ are obtained and presented for $\frac{\sigma(E_\nu)}{E_\nu}$ vs E_ν in the limit $m_l \neq 0$.

Then we have presented the results for the weak nuclear structure functions $F_{iA}(x, Q^2); (i = 1 - 3)$ in the limit $m_l = 0$, when the calculations are performed

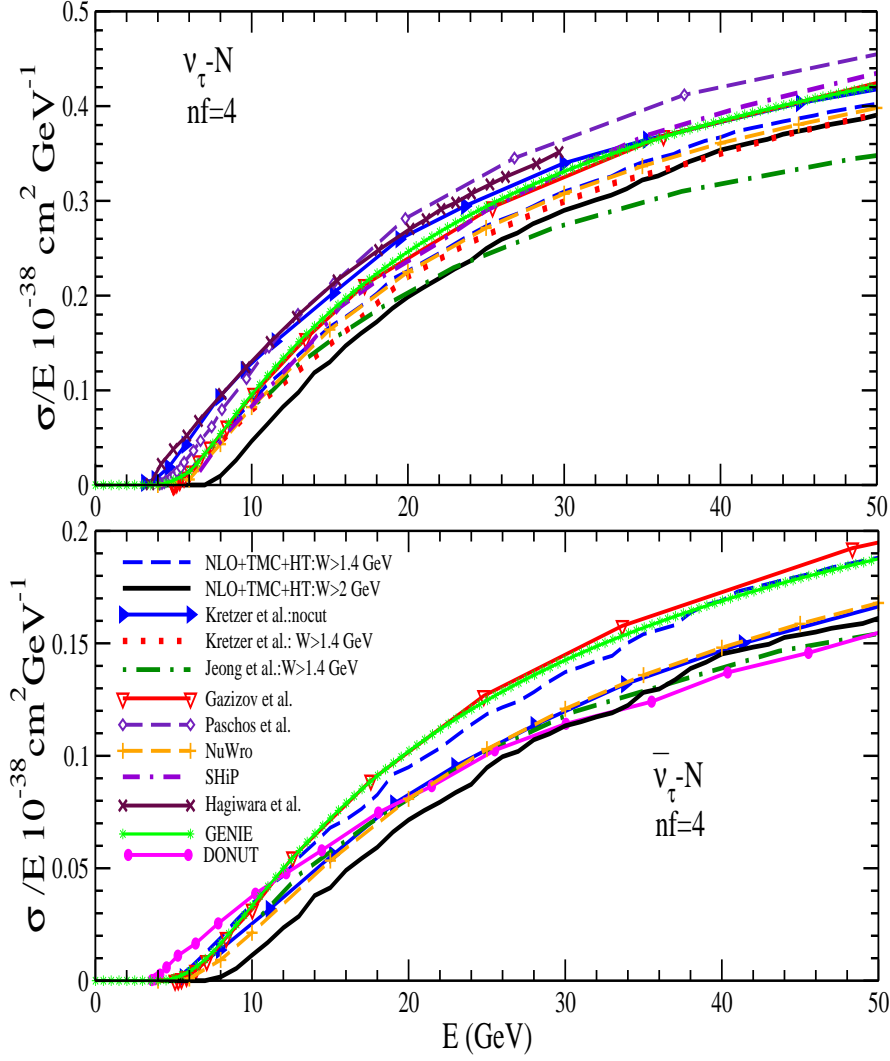


Fig. 6. $\frac{\sigma}{E}$ vs E for $\nu/\bar{\nu}_\tau$ interactions on a free nucleon target, with a center of mass energy (W) cut of 1.4 GeV (dashed line) and 2 GeV (solid line), for tau type neutrinos (Top panel) and antineutrinos (Bottom panel) with the TMC [36] and higher twist [29] effects. These results are compared with the results of various theoretical models available in the literature [37, 38, 39, 40, 41, 42, 43, 44] as well as with the Monte Carlo generators GENIE [45] and NuWro [46].

using the spectral function (SF) only. Furthermore, the contribution from the meson clouds as well as the shadowing effect are taken into account and this corresponds to the full model (Total) results. The expression of total nuclear structure functions in the full theoretical model is given by

$$F_{iA}(x, Q^2) = F_{iA,N}(x, Q^2) + F_{iA,\pi}(x, Q^2) + F_{iA,\rho}(x, Q^2) + F_{iA,shd}(x, Q^2), \quad (46)$$

where $i = 1, 2$. $F_{iA,N}(x, Q^2)$ are the weak nuclear structure functions which have contributions from the spectral function only, $F_{iA,\pi/\rho}(x, Q^2)$ take into account mesonic contributions. $F_{iA,shd}(x, Q^2)$ has contribution from the shadowing effect.

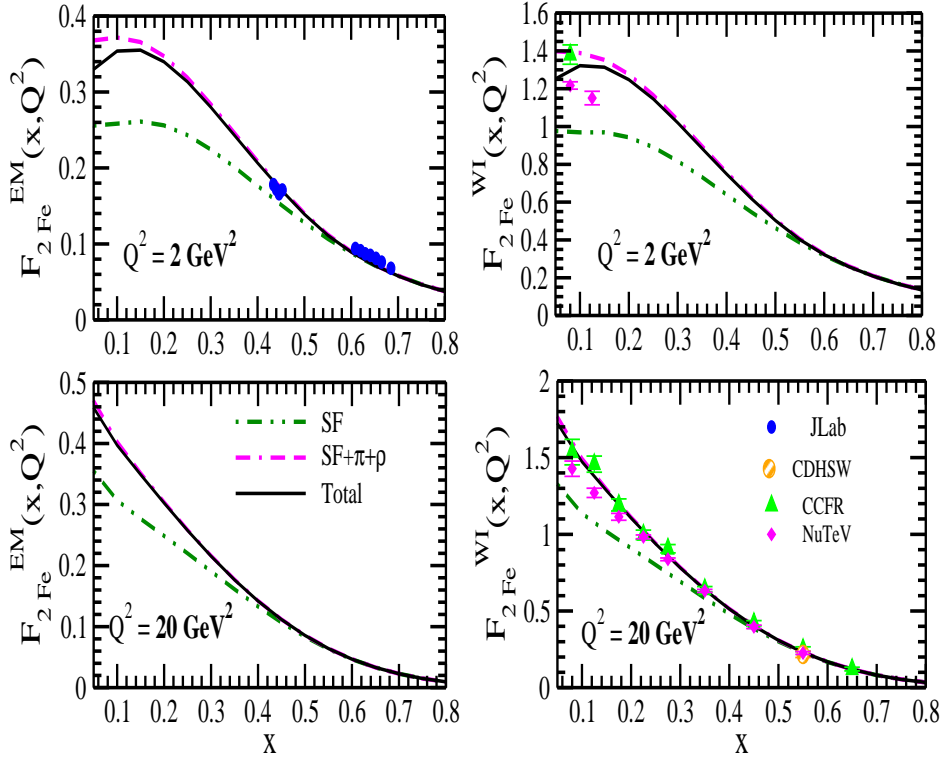


Fig. 7. Results of EM(Left panel) and Weak(Right panel) nuclear structure functions in ^{56}Fe (isoscalar) obtained using spectral function(dashed double-dotted line), including mesonic contribution(double dashed-dotted line), full model(solid line). These results are presented for different Q^2 and are compared with the available experimental data of JLab(solid circle) [47], CDHSW(semi solid circle) [11], CCFR(triangle up) [12], NuTeV(diamond) [13].

In this model, the full expression for the parity violating weak nuclear structure function $F_{3A}(x, Q^2)$ is given by,

$$F_{3A}(x, Q^2) = F_{3A,N}(x, Q^2) + F_{3A,shd}(x, Q^2). \quad (47)$$

Notice that this structure function has no mesonic contribution. The contribution to the nucleon structure function mainly comes from the valence quarks distributions. For $F_{3A,shd}(x, Q^2)$ similar definition has been used as given in Eq.(45) following the works of Kulagin et al. [17].

3.1 Nucleon Structure Function and Cross Section

In Fig. 5, the results for the free nucleon weak structure functions $2xF_{1N}(x, Q^2)$, $F_{2N}(x, Q^2)$, $xF_{3N}(x, Q^2)$, $F_{4N}(x, Q^2)$ and $2xF_{5N}(x, Q^2)$ (from the top to bottom) are shown at the two different values of Q^2 viz. $Q^2 = 2 \text{ GeV}^2$ (left panel) and $Q^2 = 5 \text{ GeV}^2$ (right panel). The nucleon structure functions are presented at NLO without the TMC effect (double dash-dotted line), with the TMC effect in 3-flavor(dash-dotted line:nf3) and 4-flavor(dotted line:nf4) schemes, with TMC and HT effects in 3-flavor(dashed line: nf3) and 4-flavor(solid line:nf4) schemes. From the figure, it may be noticed that the TMC effect is dominant in the region of high x and low Q^2 and

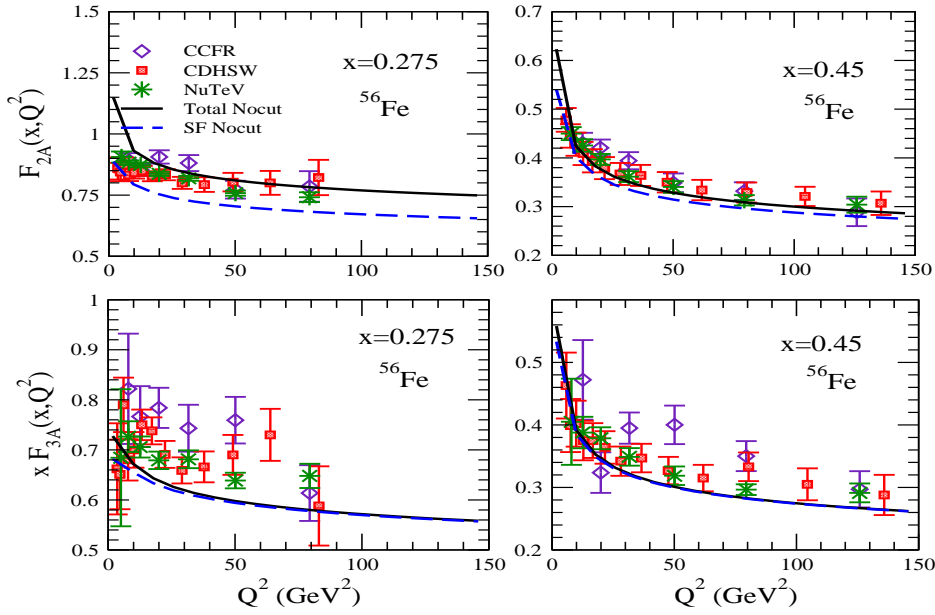


Fig. 8. Results for $F_{2A}^{\nu+\bar{\nu}}(x, Q^2)$ (top panel) and $x F_{3A}^{\nu+\bar{\nu}}(x, Q^2)$ (bottom panel) vs Q^2 are shown at $x = 0.275$ and 0.45 in ^{56}Fe . The results are obtained with the spectral function only (dashed line) and with the full model (solid line) at NNLO and are compared with the results of the available experimental data [11,12,13]. Iron is treated as an isoscalar nuclear target.

it becomes small at low x and high Q^2 . Quantitatively, the TMC effect is found to be different in $F_{2N}(x, Q^2)$ from $F_{1N}(x, Q^2)$ while the TMC effect in $F_{5N}(x, Q^2)$ is similar to the effect in $F_{2N}(x, Q^2)$. However, in the case of $F_{4N}(x, Q^2)$ the whole contribution, arises in the leading order due to the TMC effect at mid and high x . $F_{4N}(x, Q^2)$ contributes to the cross section due to the non-vanishing lepton mass when it is large, and contributes only in the region of $x \leq 0.2$. We find that at NLO, $F_{4N}(x, Q^2)$ becomes almost negligible in the region of $x > 0.2$ when TMC effect is not incorporated but with the inclusion of TMC effect a nonzero though small contribution in the region of high x and low Q^2 has been found. The difference in the results of free nucleon structure functions $F_{iN}(x, Q^2)$; ($i = 1 - 5$) evaluated at NLO with and without the TMC effect at $x = 0.3$ is 5%(3%) in $2xF_{1N}(x, Q^2)$, 2%(< 1%) in $F_{2N}(x, Q^2)$, 7%(~ 3%) in $x F_{3N}(x, Q^2)$ and 4%(~ 2%) in $2xF_{5N}(x, Q^2)$ for $Q^2 = 2(5)$ GeV^2 .

For the first three structure functions ($F_{iN}(x, Q^2)$; $i = 1 - 3$), the HT effect has also been studied. This is found to be comparatively small in $F_{1N}(x, Q^2)$ and $F_{2N}(x, Q^2)$ than in $F_{3N}(x, Q^2)$. Due to higher twist(HT) corrections, we have observed a decrease in the value of $F_{3N}(x, Q^2)$, which becomes small with the increase in Q^2 . To show the effect of massive charm on the nucleon structure functions, we have compared the results obtained with the TMC and HT effects for the three flavor of massless quarks ($n_f = 3$) with the results when additional contribution from the massive charm quark ($n_f = 4$) have also been considered. It is found that massive charm effect is almost negligible in the kinematic region of low Q^2 and high x while it increases with the increase in Q^2 and is appreciable at low x .

In Fig. 6, we have shown our results for the total scattering cross section σ/E_ν vs E_ν , for the DIS of ν_τ and $\bar{\nu}_\tau$ from the nucleons and compared them with the results

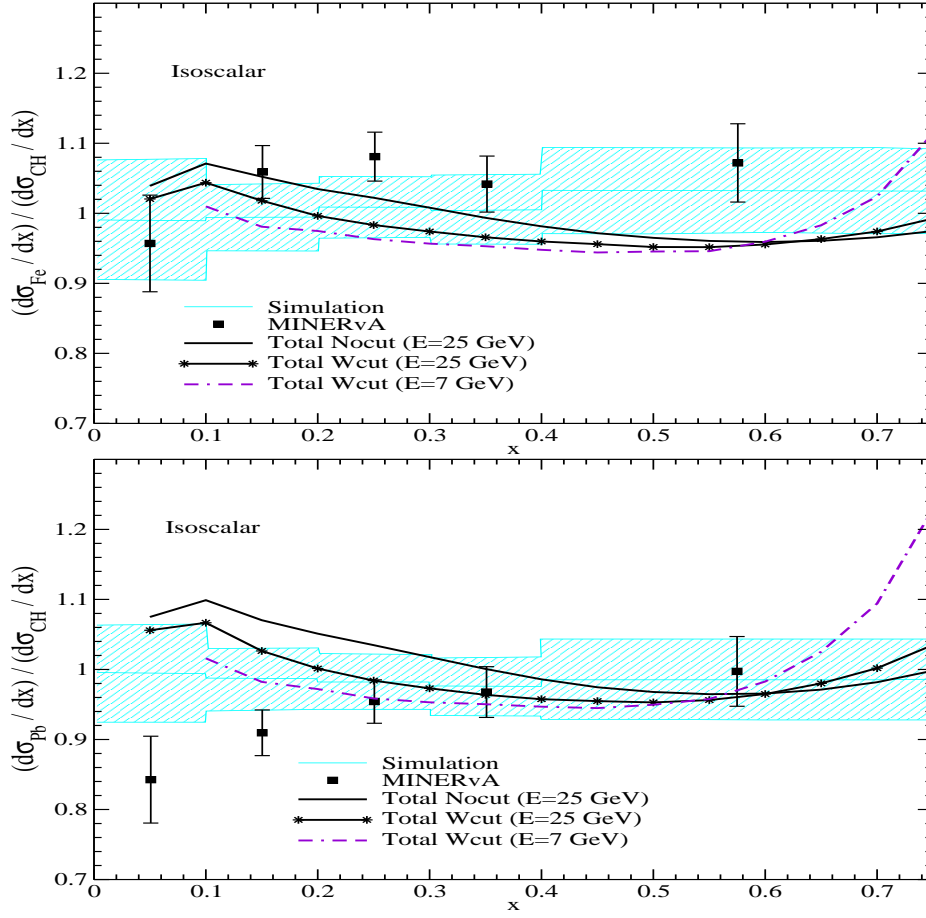


Fig. 9. $\frac{d\sigma_A/dx}{d\sigma_{CH}/dx}$ ($A = {}^{56}\text{Fe}, {}^{208}\text{Pb}$) vs x for incoming neutrino beam of energies $E = 7$ GeV and 25 GeV. The numerical results are obtained with the full model (solid line: $E = 25$ GeV, solid line with star: $E = 25$ GeV and double dash-dotted line: $E = 7$ GeV) at NNLO and are compared with the simulated results [10]. The solid squares are the experimental points of MINERvA [10]. The results are shown for the isoscalar nuclear targets.

of the different models available in the literature like that of Pashchos et al. [41] (dashed line with diamond), Kretzer et al. [37] (solid line with right triangle without a cut on W ; dotted line with a cut of $W > 1.4$ GeV), Jeong et al.[38] (dash-dotted line), Gazizov et al.[42] (solid line with down triangle), Hagiwara et al.[39] (solid line with cross symbol), Anelli et al.[44] (double dash-dotted line) and Li et al. [43] (solid line with circles) as well as with the predictions made by the Monte Carlo generator GENIE [45] and NuWro [46]. The results are presented for the two cases of cut on the center of mass energy(W), taken to be $W=1.4$ GeV(shown by dashed line) and 2 GeV(shown by the solid line). The results are presented by incorporating the target mass correction and higher twist effects at NLO in the four flavor scheme. Our results with a cut of $W = 1.4$ GeV (shown by dashed line) is in good agreement with the result of Kretzer et al. [37] (shown by the dotted line) while there are significant differences from the result of Jeong et al. [38] (shown by the dash-dotted line). Notice that the results of the total scattering cross section with the same CoM energy cut

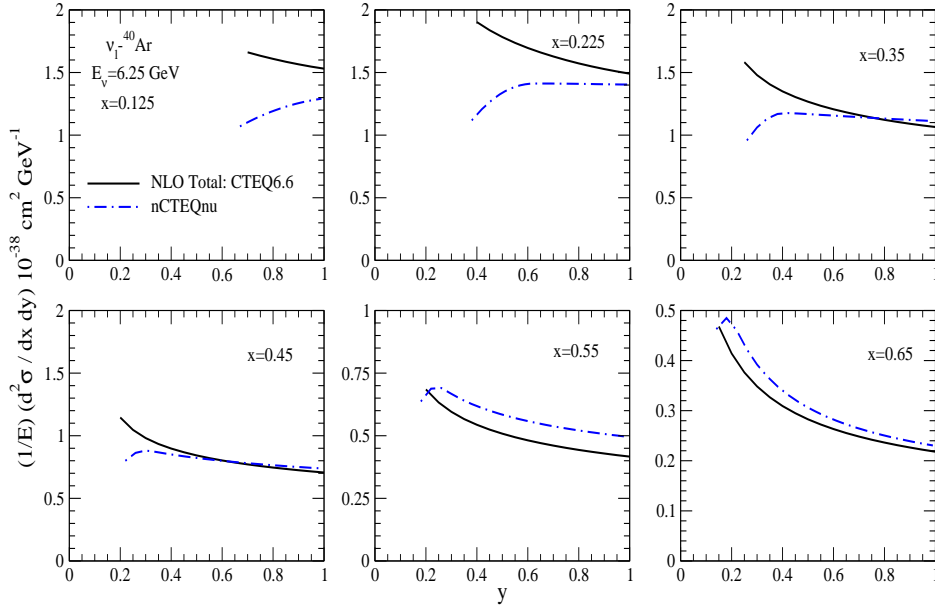


Fig. 10. Predictions for the differential scattering cross section vs y , at the different values of x for 6.25 GeV ν -Ar treated as an isoscalar target. The results are obtained with a $Q^2 \geq 1.0 \text{ GeV}^2$ cut by the Aligarh-Valencia model using CTEQ 6.6 nucleon PDFs [48] at NLO in the $\overline{\text{MS}}$ -bar scheme (solid line). The nCTEQnu nuclear PDFs [49] based prediction is the blue dash-dotted line.

reported by Kretzer and Reno [37] and Jeong and Reno [38] are also different with each other. The difference is mainly due to the choice of lower cuts on Q^2 in the evaluation of PDFs. It is important to point out that the results given by the different models [37, 38, 39, 40, 41, 42, 43, 44] have significant differences due to their choice of different kinematic conditions. Furthermore, we have observed that the dependence of the cross section on the effect of CoM energy cut is more pronounced in the case of $\bar{\nu}_\tau - N$ DIS than in $\nu_\tau - N$ DIS process. Moreover, one may also notice that the total scattering cross section is quite sensitive to the kinematic cut on the CoM energy. It implies that a suitable choice of the CoM energy cut as well as the four momentum transfer square (Q^2) cut to define the deep inelastic region and use them to calculate the nucleon structure functions, differential and total scattering cross sections is quite important. These kinematic considerations should be kept in mind while comparing the predictions of the cross sections in various theoretical models.

3.2 Nuclear Structure Function and Cross Section

In Fig. 7, we present the results for the weak nuclear structure function $F_{2A}^{Weak}(x, Q^2)$ and compare them with the electromagnetic structure function $F_{2A}^{EM}(x, Q^2)$ as a function of x for the two different values of Q^2 viz. 2 and 20 GeV^2 . In this figure, we show the curves for $F_{2A}^{EM,Weak}(x, Q^2)$ obtained using the spectral function only, also including the mesonic contribution, and finally using the full model which also includes shadowing. The use of nuclear spectral function leads to a reduction of $\sim 8\%$ at $x = 0.1$; $\sim 18\%$ at $x = 0.4$; $\sim 3\%$ at $x = 0.7$ in $F_{2A}^{EM}(x, Q^2)$ as well as in $F_{2A}^{Weak}(x, Q^2)$ nuclear structure functions as compared to the free nucleon case. The inclusion of

mesonic contributions from pion and rho mesons leads to an enhancement in these structure functions at low and medium values of x . For example, the enhancement is $\sim 30\%$ at $x=0.1$; $\sim 15\%$ at $x=0.4$; $\sim 0.3\%$ at $x=0.7$. The inclusion of shadowing effects further reduces these structure functions and are effective in low region of x (< 0.1). For example, the reduction is $\sim 10\%$ at $x=0.05$ and $\sim 5\%$ at $x=0.1$.

In Fig. 8, we present the results for the (anti)neutrino induced processes in $F_{2A}^{\nu+\bar{\nu}}(x, Q^2)$ and $x F_{3A}^{\nu+\bar{\nu}}(x, Q^2)$ vs Q^2 in ^{56}Fe by treating it as an isoscalar nuclear target at the different values of x using the full model at NNLO and compared them with the available experimental data from CCFR [12], CDHSW [11] and NuTeV [13] experiments. We find a good agreement between the theoretical results for $F_{2A}^{\nu+\bar{\nu}}(x, Q^2)$ and reasonable agreement for $F_{3A}^{\nu+\bar{\nu}}(x, Q^2)$ with the experimental data. It can be seen that the description of the nuclear medium effect in our model is able to reproduce the experimental results.

Furthermore, in Fig.9, we have presented the results for the ratio of the differential scattering cross sections, for the different nuclear targets viz. $A=^{56}\text{Fe}$ and ^{208}Pb to the hydrocarbon(CH) target i.e. $\frac{d\sigma_A/dx}{d\sigma_{CH}/dx}$ ($A=^{56}\text{Fe}, ^{208}\text{Pb}$) vs x at the two different values of neutrino energies viz. $E_\nu = 7$ GeV and $E_\nu = 25$ GeV and compared them with the corresponding experimental data of MINERvA [10]. It may be noticed that MINERvA's experimental data have large error bars and the wide band around the simulation is due to the systematic errors which shows an uncertainty up to $\sim 20\%$ [10].

Fig. 10 shows predictions for the differential scattering cross section for ν_μ induced reaction on ^{40}Ar nuclear target at $E_{\nu_\mu}=6.25$ GeV. The numerical calculations are done by using the CTEQ6.6 PDFs parameterization [48]. Our theoretical results obtained using the full model are compared with the results of nCTEQnu nPDFs [49]. As y decreases, the nPDF approach predicts lower cross sections than the theoretical approach. For high- x ($\gtrsim 0.5$), the nPDF approach and the theoretical approach both predict quite similar cross sections while for the low- x ($\lesssim 0.3$) region the nPDF approach predicts a lower cross section than our theoretical model.

3.3 Nonisoscality Effect

For a nonisoscality nuclear target like ^{56}Fe and ^{208}Pb , where $(A - Z) > Z$, we obtain the normalized spectral function to the proton (S_h^p) and neutron (S_h^n) numbers (Eqs.34, 32 and 33). For details please see the discussion in Ref.[4]. In Fig.11, we have presented the results for the ratios of nuclear structure functions $\frac{F_{iA}(x, Q^2)}{F_{iA'}(x, Q^2)}$; ($i = 1, 2, 3$; $A = ^{56}\text{Fe}, ^{208}\text{Pb}$ and $A' = ^{12}\text{C}$) vs x at $Q^2 = 5$ GeV². The present numerical results are obtained by using the full model at NNLO and treating iron and lead to be isoscalar as well as nonisoscality nuclear targets. We find that the ratios $\frac{F_{iFe}(x, Q^2)}{F_{iC}(x, Q^2)}$ and $\frac{F_{iPb}(x, Q^2)}{F_{iC}(x, Q^2)}$ deviate from unity in the entire range of x which implies that nuclear medium effects are A dependent, and the medium effects become more pronounced with the increase in the nuclear mass number. This enhancement in the ratio is more at high x .

4 Summary

1. The inclusion of perturbative and nonperturbative effects is quite important in the evaluation of nucleon structure functions. These effects are both x and Q^2 dependent.

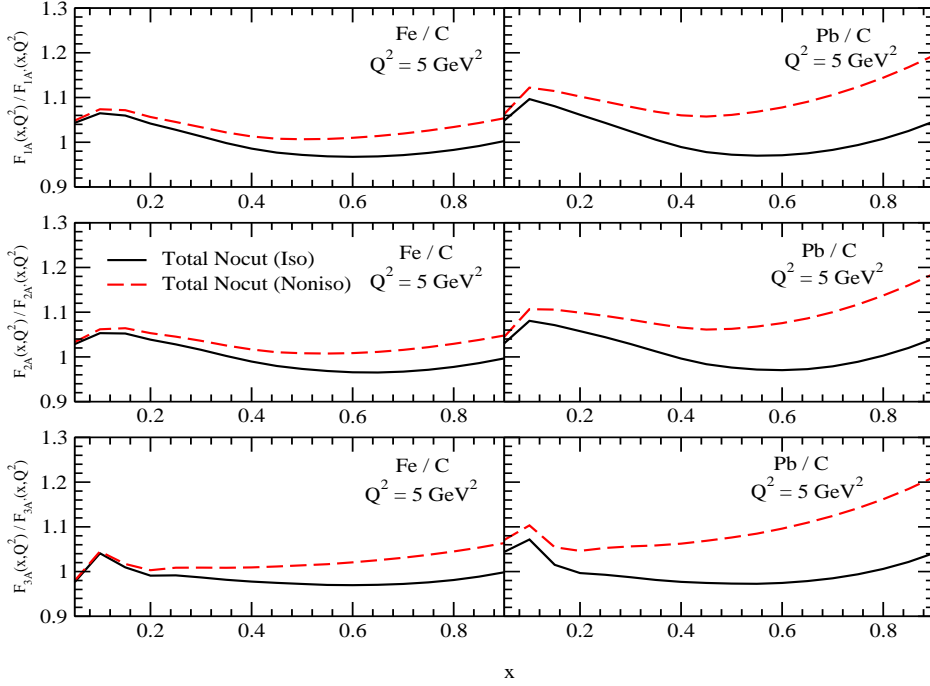


Fig. 11. $\frac{F_{iA}(x, Q^2)}{F_{iA'}(x, Q^2)}$; ($i = 1 - 3$; $A = {}^{56}\text{Fe}$, ${}^{208}\text{Pb}$; $A' = {}^{12}\text{C}$) vs x are shown at $Q^2 = 5$ GeV^2 . The results are obtained using the full model at NNLO by treating ${}^{56}\text{Fe}$, ${}^{208}\text{Pb}$ to be isoscalar (solid line) as well as nonisoscalar (dashed line) nuclear targets.

2. The difference in the results of all the free nucleon structure functions $F_{iN}(x, Q^2)$; ($i = 1 - 5$) evaluated at NLO with and without the TMC effect is non-negligible. In the case of $F_{4N}(x, Q^2)$ this difference is quite large when TMC effect is considered, specially at mid and high x . The higher twist (HT) effect has not much effect on $F_{1N}(x, Q^2)$ and $F_{2N}(x, Q^2)$, but affects $F_{3N}(x, Q^2)$. We find that the difference due to HT effect is somewhat larger for $F_{3N}(x, Q^2)$ at low x and low Q^2 . With the increase in x the effect of HT increases.
3. The total cross section σ for ν_τ and $\bar{\nu}_\tau$ interactions on the free nucleon target shows significant dependence on the model used to calculate the nucleon structure functions which implies that there are uncertainties even at the level of free nucleon level and more work is needed.
4. NME in $F_{2A}^{EM}(x, Q^2)$ and $F_{2A}^{Weak}(x, Q^2)$ in iron nucleus are almost the same for x i.e $x > 0.3$, but are different in small x region ($x < 0.3$). However, this difference is found to be very small for isoscalar nuclei, and is similar to the case of free nucleon.
5. The nuclear structure functions obtained with spectral function only are suppressed as compared to the free nucleon case in the entire region of x . Whereas, the inclusion of mesonic contributions results in an enhancement in the nuclear structure functions in the low and intermediate region of x . Mesonic contributions are observed to be more pronounced with the increase in mass number and they decrease with the increase in x and Q^2 . The results for the nuclear structure functions $F_{2A}^{Weak}(x, Q^2)$ and $F_{3A}^{Weak}(x, Q^2)$ with the full theoretical model show good agreement with the experimental data of CCFR [12], CDHSW [11] and NuTeV [13] especially at high x and high Q^2 .

6. The present theoretical results for the ratio $\frac{d\sigma_A^{Weak}/dx}{d\sigma_{CH}^{Weak}/dx}$ ($A = {}^{56}\text{Fe}, {}^{208}\text{Pb}$) when compared with the different phenomenological models and the recent MINERvA's experimental data on $\nu_l - A$ scattering, imply that a better understanding of nuclear medium effects is required for the $\nu_l(\bar{\nu}_l)$ -nucleus deep inelastic scattering process.
7. We find the non-isoscalarity effect to be non-negligible which increases with the non-isoscalarity $\delta(= \frac{N-Z}{A})$ and x .
8. Predictions are also made for $\nu_\mu(\bar{\nu}_\mu)$ interactions on ${}^{40}\text{Ar}$ that may be useful in analyzing the experimental results of DUNE [20].

Acknowledgment

F. Zaidi is thankful to the Council of Scientific & Industrial Research (CSIR), India, for providing the research associate fellowship with award letter no. 09/112(0622)2K19 EMR-I. I. Ruiz Simo acknowledges support from Spanish Ministry of Science and ERDF under contract FIS2017-85053-C2-1P, and from Junta de Andalucia through grant No FQM-225.

References

1. H. Haider, I. R. Simo, M. Sajjad Athar and M. J. V. Vacas, Phys. Rev. C **84**, 054610 (2011).
2. H. Haider, I. Ruiz Simo and M. Sajjad Athar, Phys. Rev. C **85**, 055201 (2012).
3. H. Haider, F. Zaidi, M. Sajjad Athar, S. K. Singh and I. Ruiz Simo, Nucl. Phys. A **955**, 58 (2016).
4. F. Zaidi, H. Haider, M. Sajjad Athar, S. K. Singh and I. Ruiz Simo, Phys. Rev. D **99**, 093011 (2019).
5. F. Zaidi, H. Haider, M. Sajjad Athar, S. K. Singh and I. Ruiz Simo, Phys. Rev. D **101**, 033001 (2020).
6. V. Ansari, M. Sajjad Athar, H. Haider, S. K. Singh and F. Zaidi, Phys. Rev. D **102**, 113007 (2020).
7. M. Sajjad Athar and J. G. Morfin, J. Phys. G **48**, 034001 (2021).
8. C. G. Callan, Jr. and D. J. Gross, Phys. Rev. Lett. **22**, 156 (1969).
9. C. H. Albright and C. Jarlskog, Nucl. Phys. B **84**, 467 (1975).
10. J. Mousseau *et al.* [MINERvA Collaboration], Phys. Rev. D **93**, no. 7, 071101 (2016).
11. J. P. Berge *et al.*, Z. Phys. C **49**, 187 (1991).
12. E. Oltman *et al.*, Z. Phys. C **53**, 51 (1992).
13. M. Tzanov *et al.* [NuTeV Collaboration], Phys. Rev. D **74**, 012008 (2006).
14. K. Kovarik *et al.*, Phys. Rev. D **93**, 085037 (2016).
15. M. Sajjad Athar, I. Ruiz Simo and M. J. Vicente Vacas, Nucl. Phys. A **857**, 29 (2011).
16. S. A. Kulagin and R. Petti, Phys. Rev. D **76**, 094023 (2007).
17. S. A. Kulagin and R. Petti, Nucl. Phys. A **765**, 126 (2006).
18. E. Marco *et al.*, Nucl. Phys. A **611**, 484 (1996).
19. P. Fernandez de Cordoba and E. Oset, Phys. Rev. C **46**, 1697 (1992).
20. B. Abi *et al.* [DUNE Collaboration], arXiv:1807.10327 [physics.ins-det].
21. Y. L. Dokshitzer, Sov. Phys. JETP **46**, 641 (1977).
22. V. N. Gribov and L. N. Lipatov, Sov. J. Nucl. Phys. **15**, 438 (1972).
23. G. Altarelli and G. Parisi, Nucl. Phys. B **126**, 298 (1977).
24. L. N. Lipatov, Sov. J. Nucl. Phys. **20**, 94 (1975) [Yad. Fiz. **20**, 181 (1974)].
25. L. A. Harland-Lang *et al.*, Eur. Phys. J. C **75**, 204 (2015).
26. J. A. M. Vermaseren *et al.*, Nucl. Phys. B **724**, 3 (2005).
27. S. Moch, J. A. M. Vermaseren and A. Vogt, Phys. Lett. B **606**, 123 (2005).

28. S. Moch, J. A. M. Vermaseren and A. Vogt, Nucl. Phys. B **813**, 220 (2009).
29. M. Dasgupta and B. R. Webber, Phys. Lett. B **382**, 273 (1996).
30. I. Schienbein *et al.*, J. Phys. G **35**, 053101 (2008).
31. H. Haider, F. Zaidi, M. Sajjad Athar, S. K. Singh and I. Ruiz Simo, Nucl. Phys. A **943**, 58 (2015).
32. H. DeVries, C. W. DeJager, C. DeVries, Atomic Data and Nuclear Data Tables **36**, 495 (1987).
33. H. Haider, M. Sajjad Athar, S. K. Singh and I. R. Simo, J. Phys. G **44**, 045111 (2017).
34. H. Haider, I. Ruiz Simó, M. Sajjad Athar and M. Vicente Vacas, DAE Symp. Nucl. Phys. **56**, 868 (2011).
35. M. Gluck *et al.*, Z. Phys. C **53**, 651 (1992).
36. S. Kretzer and M. Reno, Phys. Rev. D **69**, 034002 (2004).
37. S. Kretzer and M. H. Reno, Phys. Rev. D **66**, 113007 (2002).
38. Y. S. Jeong and M. H. Reno, Phys. Rev. D **82**, 033010 (2010).
39. K. Hagiwara, K. Mawatari and H. Yokoya, Nucl. Phys. B **668**, 364 (2003).
40. J. Conrad, A. de Gouvea, S. Shalgar and J. Spitz, Phys. Rev. D **82**, 093012 (2010).
41. E. A. Paschos and J. Y. Yu, Phys. Rev. D **65**, 033002 (2002).
42. A. Gazizov *et al.*, EPJ Web of Conferences 116, 08003 (2016).
43. Z. Li *et al.* [Super-Kamiokande Collaboration], Phys. Rev. D **98**, 052006 (2018).
44. M. Anelli *et al.* [SHiP Collaboration], arXiv:1504.04956 [physics.ins-det].
45. private communication.
46. private communication.
47. V. Mamyán, arXiv:1202.1457 [nucl-ex].
48. P. M. Nadolsky *et al.*, Phys. Rev. D **78**, 013004 (2008);
<http://hep.pa.msu.edu/cteq/public>.
49. J. G. Morfin, private communication.